Journal of Solid State Chemistry 182 (2009) 1–7

Contents lists available at ScienceDirect

Journal of Solid State Chemistry

journal homepage: www.elsevier.com/locate/jssc

Actinide incorporation in a zirconia based pyrochlore $(Nd_{1.8}An_{0.2})Zr_2O_{7+x}$ (An = Th, U, Np, Pu, Am)

Catharina Nästren [a,b], Regis Jardin [a], Joseph Somers [a], Marcus Walter [a,*], Boris Brendebach [c]

[a] European Commission, Joint Research Centre, Institute for Transuranium Elements, P.O. Box 2340, D-76125 Karlsruhe, Germany
[b] Nuclear Chemistry at the Department of Chemical and Biological Engineering, Chalmers University of Technology, SE-412 96 Göteborg, Sweden
[c] Forschungszentrum Karlsruhe, Institut für Nukleare Entsorgung (INE), P.O. Box 3640, D-76021 Karlsruhe, Germany

ARTICLE INFO

Article history:
Received 18 June 2008
Received in revised form
22 September 2008
Accepted 29 September 2008
Available online 9 October 2008

Keywords:
Minor actinides
Transmutation
Nuclear waste disposal
Conditioning
Pyrochlore
Zirconia
EXAFS

ABSTRACT

Actinides (thorium, uranium, neptunium, plutonium, and americium) were infiltrated into a porous $Nd_{1.8}Zr_2O_{6.7}$ matrix, prepared by gel-supported precipitation. $(Nd_{1.8}An_{0.2})Zr_2O_{7+x}$ pyrochlores were formed after sintering in Ar/H_2 and the pyrochlore structure remains during oxidation at 800 °C in air. X-ray diffraction reveals a linear relationship between the pyrochlore lattice parameter and the ionic radii of the actinides. EXAFS measurements on actinide L_3-edge show a split shell of nearest neighbour oxygen atoms similar to that surrounding of Nd. The actinide–oxygen bond distances decrease with the actinide ionic radii, which verifies that these actinides adopt the Nd site in the $(Nd_{1.8}An_{0.2})Zr_2O_{7+x}$ pyrochlore. The oxidation susceptibility of Np is related to the availability of oxygen vacancies and in contrast to stabilised zirconia Np(V) can be obtained in zirconia based pyrochlore.

1. Introduction

The long-term radiotoxicity of spent nuclear fuel is dominated by plutonium and the minor actinides (MA = Np, Am, Cm). To reduce the amount of these elements for final disposal, considerable effort is made to develop host matrices to transmute these actinides in nuclear reactors or accelerator driven systems. In a complementary strategy, matrices with high radiation resistance and aqueous durability are of interest for a safe disposal of Pu and MA (i.e. conditioning). Due to their advantageous properties (thermal stability, low cross section for neutrons, aqueous durability, chemical flexibility), zirconia based compounds are considered for both the transmutation [1–3] and conditioning [4,5] strategies to deal with Pu and MA in spent nuclear fuel.

Zirconia, which is monoclinic at room temperature and ambient pressure, can be stabilised in tetragonal and cubic forms by the addition of large trivalent atoms such as the rare earth elements (REE). The cubic stabilised zirconia $(Zr,REE)O_{2-x}$ crystallises in the (defect) fluorite structure, where the metal and oxygen atoms are randomly distributed. An ordered derivative of cubic stabilised zirconia is the pyrochlore structure, $A_2Zr_2O_7$, which is formed in a narrow region of the A_2O_3–ZrO_2 phase diagram for trivalent elements whose atomic radius lies in a specific range (1.05–1.16 Å). Such trivalent atoms, A(III), include La–Gd and Pu–Cf [6,7]. There are two different sites for both cations and anions in the pyrochlore structure which has a unit cell almost twice that of the fluorite structure. The zirconium atoms are coordinated by six oxygen atoms (48*f*) at a distance of about 2.1 Å, whereas the eight oxygen atoms surrounding the A(III) atoms are split into two configurations with two O atoms (8*b*) with a shorter (~2.3 Å) and six O atoms (48*f*) with a longer (~2.6 Å) bond length. The crystallographic 8*a* oxygen site is unoccupied [8]. Another, more ordered derivate of the defect fluorite structure is zirconolite, $CaZrTi_2O_7$, which is also considered as conditioning matrix for actinides [5].

As the actinide content in pure $An_2Zr_2O_7$ is too high for either transmutation or conditioning purposes, the rare earth based pyrochlore seems to be a suitable host matrix for Pu and MA [7,9,10]. Because of the similar ionic radii of Am(III) and Nd(III), the pyrochlore $Nd_2Zr_2O_7$ is of particular interest for these applications [3]. Dilution of the actinides in this compound can be achieved by use of compounds of the form $(Nd_{2-y}An_y)Zr_2O_{7+x}$. The composition $y = 0.2$ is chosen so that the equivalent compound without the actinide, An, also lies above the lower pyrochlore limit in the phase diagram.

* Corresponding author. Fax: +49 7247 951 566.
E-mail address: marcus.walter@ec.europa.eu (M. Walter).

0022-4596/$ - see front matter © 2008 Elsevier Inc. All rights reserved.
doi:10.1016/j.jssc.2008.09.017

Substitution of Nd in $Nd_2Zr_2O_7$ with Am and Pu and their α-decay daughters Np and U will affect the local structure of the pyrochlore as the actinide dopant and their decay/transmutation products are different from Nd in ionic radii and valency. The local structure of actinides in $(Nd_{1.8}An_{0.2})Zr_2O_{7+x}$ can be probed selectively by X-ray absorption spectroscopy. The X-ray absorption near edge structure (XANES) provides information mainly on the actinide oxidation state and the Zr site symmetry, whereas local structure parameters (e.g. bond lengths) can be obtained from extended X-ray absorption fine structure (EXAFS). A combination of XANES and EXAFS has been used to identify the local structure in stabilised zirconia [11,12] and pyrochlores [11,13]. The local structure of incorporated uranium and plutonium in titanate based conditioning matrices [14–17], and U [18] and Am [19] in cubic stabilised zirconia has been reported.

The aim of the present work is to investigate the incorporation of Th, U, Np, Pu, and Am in a $(Nd_{1.8}An_{0.2})Zr_2O_{7+x}$ pyrochlore and to characterise the local structure of these actinides, in various oxidation states, using X-ray absorption spectroscopy.

2. Experimental

2.1. Sample preparation

The actinide doped pyrochlores were prepared by infiltration of porous $Nd_{1.8}Zr_2O_{6.7}$ beads with actinide nitrate solutions [1]. The $Nd_{1.8}Zr_2O_{6.7}$ beads were obtained using a gel-supported precipitation route. This process route ensures that the Nd:Zr ratio is identical for all samples. Briefly, solutions of neodymium nitrate and zirconyl chloride (both Alfa Aesar 99.9%) were mixed in the desired stoichiometry. An organic thickener (Methocel, Dow Chemicals) was added to increase the viscosity of the solution. The solution was dispersed and the droplets were collected in an ammonia bath, where hydrolysis causes the droplet to particle conversion. After washing and drying, the beads were calcined at 800 °C in air (4 h). This is an important route for the production of these materials, as the particles are dust free, enabling simplified, clean industrial processing. The open porosity available for the actinide infiltration was about 45 vol%. X-ray diffraction of this precursor material reveals a less crystalline material with a fluorite structure and a mean crystallite size of 8 nm.

These porous beads were then infiltrated with La, Nd, ^{232}Th, $U(VI)_{depleted}$, ^{237}Np, Pu (76% ^{238}Pu, 20% ^{239}Pu, 3% ^{240}Pu), and ^{241}Am to produce $(Nd_{1.8}A_{0.2})Zr_2O_7$. The material was then dried and calcined at 800 °C in Ar/H_2. Pellets were pressed (500 MPa) and sintered in Ar/H_2 at 1650 °C (30 h, metal furnace). X-ray diffraction revealed single pyrochlore phases, except for $(Nd_{1.8}Th_{0.2})Zr_2O_7$ where free ThO_2 was detected. This sample was milled, pressed and again sintered for 24 h, but traces of ThO_2 (~1%) were still present after a total of 90 h at 1650 °C. In the case of the redox-sensitive elements U, Np, Pu, and Am, part of the material was annealed at 800 °C in air (24 h) to oxidise the actinides.

2.2. Sample analysis

Powder X-ray diffraction patterns were recorded in Bragg–Brentano geometry using a Bruker D8 diffractometer (Cu-$K\alpha$1, Ge monochromator) equipped with a position sensitive detector (Vantec). The 2θ scanning range was from 20° to 120° with incremental steps of 0.0085°. The lattice parameter of the $Fd\bar{3}m$ pyrochlore structure was refined using the Fullprof suite [20].

The Pu and Am content in the solids was determined by calorimetry. The Np content was measured by γ-spectroscopy using the Am sample for efficiency calibration. The obtained values (Np 7.27, Pu 7.80, Am 6.89 wt%) are close to the planned value of 7.9–8.0 wt%. The larger difference in case of Am might be due to uncertainties in the solution concentration used for the infiltration, as slight evaporation can occur.

2.3. EXAFS measurements

The $(Nd_{2-x}An_x)Zr_2O_7$ samples were milled, mixed with BN or dried MgO (Np, Pu, and Am samples) and pressed into disks. The X-ray absorption (XAS) measurements were performed at the INE-Beamline [21] at the Ångströmquelle Karlsruhe, ANKA. A pair of Ge(422) crystals (Si(111) in case of Nd L_3-edge) was used in the double-crystal monochromator. Two Rh-coated mirrors ensured the rejection of higher harmonics at this beamline. The XAS spectra at the Zr *K*-edge and U, Np, Am L_3-edges were recorded in transmission mode at room temperature. The Pu L_3 (18057 eV) coincides with the Zr *K*-edge (17998 eV). Therefore no good quality data could be recorded for Pu. The Nd L_3-edge (6201 eV) was measured only for $Nd_2Zr_2O_7$ as the radiation protection sealing of the active samples cause very high absorption of photon's recorded in the Nd L_3-edge region. The Nd L_3-edge spectra were measured in fluorescence mode using a five element LEGe solid state detector (Canberra).

The EXAFS oscillations were extracted according to standard procedures using WINXAS [22]. The threshold energy, E_0, was defined as the first maximum of the first derivate XANES. Spherical 8 Å cluster of atoms with the Cartesian coordinates of $(Nd_{1.8}A_{0.2})Zr_2O_7$ (A = U, Np, Am) [8] were used for the calculation of theoretical phase shifts, $\delta(k)$, and backscattering amplitude functions, $F(k)$, (FEFF8 [23]). The amplitude reduction factor was held constant at 1.0 for the EXAFS fits. The shift in threshold energy, ΔE_0, was varied as a global parameter in the fit procedure. The EXAFS data were refined in *R*-space (Zr: 0.5–4.0 Å, Nd, *An*: 0.5–5.5 Å) of the Fourier transformed k^3-weighted $\chi(k)$ data. The *k*-range was 2.8–10.7 $Å^{-1}$ for Zr and approximately 2.5–10 $Å^{-1}$ for Nd, *An*, depending on spectra quality.

3. Results and discussion

3.1. X-ray diffraction

Due to the thermal treatment in reducing (Ar/H_2) and oxidising atmosphere (air), U, Np, Pu, and Am are obtained in different oxidation states. The oxidation states of La(III), Nd(III), and Th(IV) are independent of the sinter conditions. For the remaining actinides the oxidation states obtained under reducing conditions (Ar/H_2) are U(IV), Np(IV), Pu(III), and Am(III) [24]. The ionic radii of Pu(III) and Am(III) are such that they form pyrochlores with zirconia. Under oxidising conditions, as applied in this work, dioxides of Pu and Am will form and the oxidised $(Nd_{1.8}A_{0.2})Zr_2O_7$ samples contain Pu(IV) and Am(IV). UO_2 easily accommodates oxygen and several stable compounds with intermediate oxidation state are observed between UO_2 and UO_3. U_3O_8 forms when UO_2 is oxidised in air at 800 °C [24]. Np_2O_5 is the binary Np oxide with the highest Np oxidation state. Due to the fact that the $(Nd_{1.8}U_{0.2})Zr_2O_{7+x}$ lattice parameter is smaller after oxidation than that for the Np sample, the U valency is most likely higher than the Np valency. Based on their general chemical behaviour mixed U(V)–U(VI) and Np(V) are assumed as the oxidised pyrochlores (see below for further discussion).

Fig. 1 shows the $(Nd_{1.8}An_{0.2})Zr_2O_{7+x}$ pyrochlore lattice parameter as function of the actinide dopant ionic radii in eightfold coordination [25,26]. The Np(V) ionic radius (0.88 Å) was derived from the Pa(V) ionic radius [25] using the radii of tetravalent

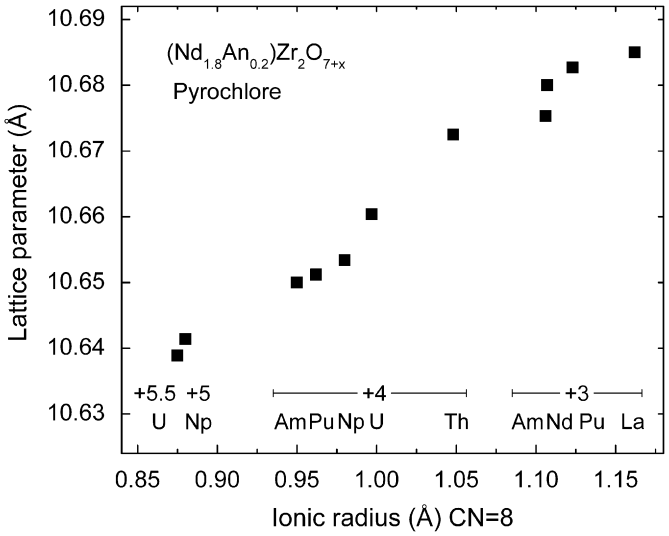

Fig. 1. $(Nd_{1.8}An_{0.2})Zr_2O_{7+x}$ pyrochlore lattice parameter depending on the actinide, La, and Nd ionic radii in eightfold coordination [25,26]. The ionic radius of Np(V) was estimated as 0.88 Å.

actinides in eightfold coordination for extrapolation. As can be seen from Fig. 1, the lattice parameter correlates linearly with the ionic radii of the dopant ion. This indicates that the $Nd_2Zr_2O_7$ pyrochlore is able to accommodate these actinides. In addition, the nearly linear correlation supports the assignment of the actinide oxidation states, where La(III) and Th(IV) serve essentially as "fixed points" as their valence does not change in Ar/H_2 or air. Small deviations from this line could be attributed to small differences in sample stoichiometry, i.e. the infiltrated *An* metal content.

3.2. Self-irradiation effects on crystal structure

The lattice parameter of the Am and Pu doped pyrochlore was monitored as function of the received dose, i.e. storage time, and the refined values are shown in Fig. 2. The pyrochlore lattice swells immediately after sintering. The measured lattice parameter of the Pu(III) doped pyrochlore starts to decrease slowly after several months of storage ($\sim 4\times10^{17}$ α-decays g^{-1}). This could be an artiefact due to partial oxidation of the Pu(III) caused by oxygen impurities in the N_2 glove box atmosphere. The Am(III) sample seems to be less susceptible to oxidation. The lattice parameter of the Pu(IV) and Am(IV) samples exhibit similar swelling and a maximum swelling of $V/V_0 = 0.3\%$ is reached after 1×10^{18} α-decays g^{-1} (one year storage of Pu(IV) sample). This is significantly smaller than that observed for Cm doped titanate pyrochlore (5–6% [27]), but is comparable to the swelling behaviour of PuO_2 (0.97% [27]). With increasing α-dose the diffraction peaks indicative of the pyrochlore structure (e.g. (311), (331), (333), (531)) disappear, whereas the peaks belonging to the fluorite structure (e.g. (222), (400), (440), etc) are less affected in intensity. Similar findings are reported for ion beam irradiation of $Gd_2Zr_2O_7$ [4,28]. To quantify this pyrochlore to fluorite transformation, the intensity of peaks characteristic of the pyrochlore structure were normalised to the strongest peak (222), which corresponds to the (111) of the fluorite structure. The natural logarithm of the (331)/(222) ratio is plotted for the Pu(III) and Pu(IV) doped samples in Fig. 2. A linear fit, corresponding to first order reaction, was applied and the half-life for the pyrochlore to fluorite transformation corresponds to 6.4×10^{17} α-decays g^{-1} (197 d) for Pu(III) and 6.8×10^{17} α-decays g^{-1} (209 d) for Pu(IV) doped pyrochlore, respectively. The normalised peak intensity

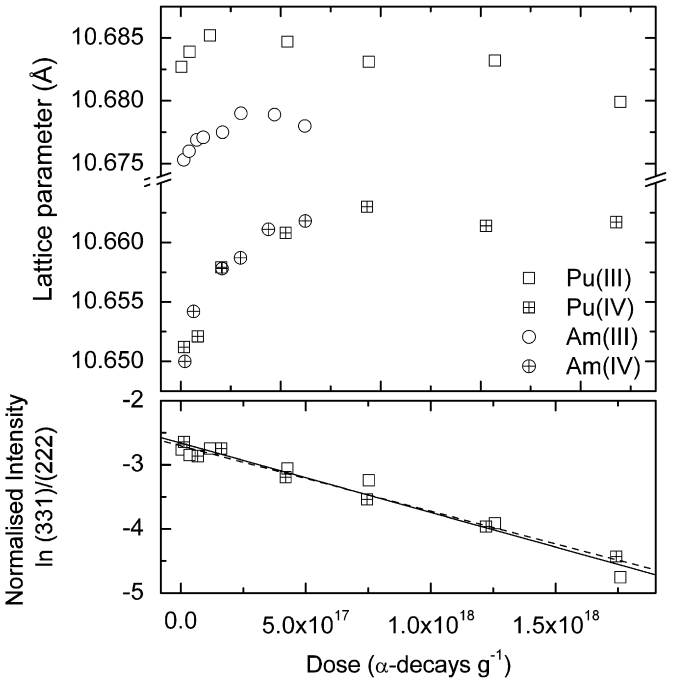

Fig. 2. Lattice parameter of aged Am, Pu doped pyrochlore as function of dose (top). Logarithm of the normalised (331)/(222) peak intensity ratio of the $(Nd_{1.8}Pu_{0.2})Zr_2O_{7+x}$ pyrochlore (below). The linear fits corresponds to first order reaction with half-live corresponding to 6.4×10^{17} α-decays g^{-1} (197 d) for Pu(III) (solid line) and 6.8×10^{17} α-decays g^{-1} (209 d) for Pu(IV) (dashed line) doped pyrochlore.

ratios of the Am samples follow the same trend; however, the accumulated dose is too small to quantify this effect. The loss of cation and anion ordering during the pyrochlore to fluorite transformation could be a reason for the low swelling observed for the pyrochlore samples. The rare earth zirconia pyrochlore lattice has a lower density than the REE stabilised zirconia with (defect) fluorite structure [11,29]. Therefore, the swelling induced by self-radiation might be compensated by the concomitant densification caused by the loss in cation and anion ordering. Further X-ray diffraction measurements are ongoing to evaluate the effects of radiation damage in these materials.

3.3. XANES

The normalised XANES spectra at the U, Np, and Am L_3-edge are shown in Fig. 3 for reduced and oxidised samples. In addition, the Zr *K*-edge XANES is provided for $Nd_2Zr_2O_7$, oxidised $(Nd_{1.8}U_{0.2})Zr_2O_{7+x}$, and $(Zr_{0.84}Y_{0.16})O_{1.92}$. The L_3-edge XANES spectra of the reduced U, Np, and Am doped pyrochlore are similar in shape. In case of U, the edge position is essentially the same as for the UO_2 reference, proving that uranium in $(Nd_{1.8}U_{0.2})Zr_2O_{7+x}$ is tetravalent when sintered in Ar/H_2. After oxidation at 800 °C in air, the ionisation energy of these actinide L_3-edges shifts to higher energies. Furthermore, the white line peak broadens significantly and becomes asymmetric. Since an asymmetric white line influences the determination of the threshold energy position from the inflection point [30], the position of the white line was used to estimate the shift in ionisation energy upon oxidation (Fig. 3). The shift is highest for U (+3.5 eV) and the XANES data are similar in position to that of U_3O_8 ($O/U \cong 2.67$). This agrees with an O/U increase of 0.77 determined by oxidation of the U(IV) doped pyrochlore in a thermobalance and a mixed U(V)–U(VI) valancy close to +5.5 can be assumed for the oxidised $(Nd_{1.8}U_{0.2})Zr_2O_{7+x}$ pyrochlore. The

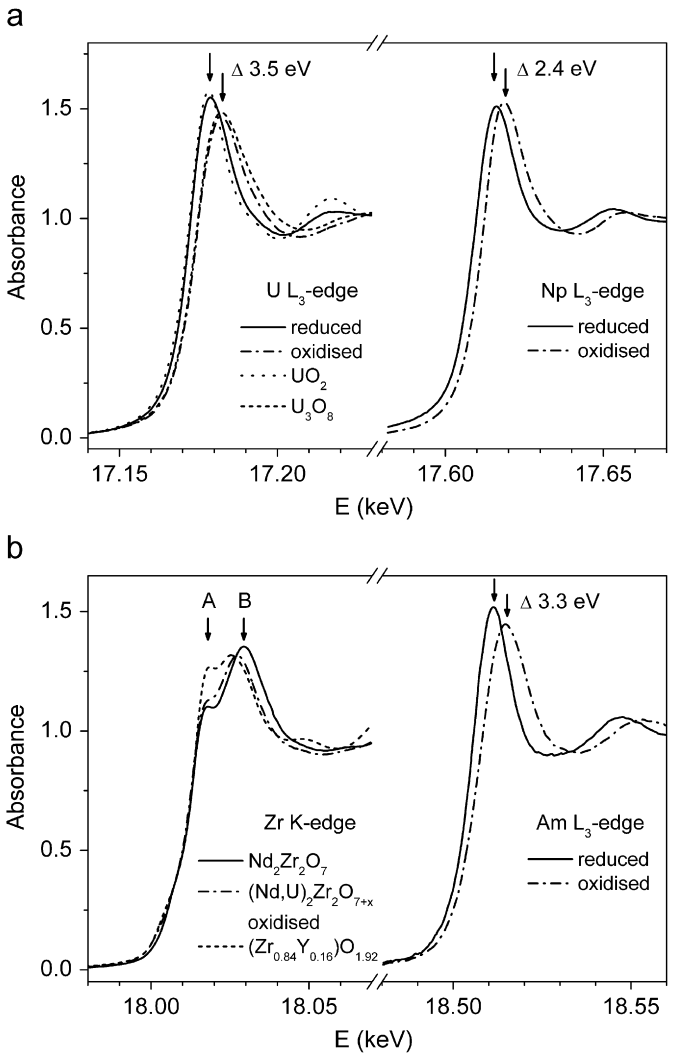

Fig. 3. XANES of U, Np, Am, and Zr in the $(Nd_{1.8}An_{0.2})Zr_2O_{7+x}$ pyrochlore.

shift is somewhat smaller for Np (2.5 eV), and in comparison with ternary uranium oxides [30] it is in the order of one valence unit, indicative that Np(IV) is oxidised to Np(V). The Am XANES are similar to those of Am(III) and Am(IV) in $(Zr,Y,Am)O_{2-x}$ [19], and by analogy Am(III) and Am(IV) are present in the reduced and oxidised $(Nd_{1.8}Am_{0.2})Zr_2O_{7+x}$.

Actinides in the oxidation state +5 and +6 often form oxycations (actinyl: NpO_2^+, UO_2^{2+}) with two oxygen atoms at a short distance of approximately 1.8 Å. The L_3-edge ionisation energy of actinyl ions is close or even lower than the energies of the +4 actinide cations [31]. Multiple scattering (MS) along this actinyl-group causes a XANES feature approximately 15 eV above the white line [32], which is not observed for the oxidised U and Np doped pyrochlore samples. The absence of this MS feature and the shift to higher absorption energies indicate that such short U–O and Np–O bonds are not formed and exclude the presence of such actinyl groups in these oxidised pyrochlores.

The Zr *K*-edge is sensitive to the change in the local Zr structure with increasing actinide valence, i.e. oxygen content in the $(Nd_{1.8}An_{0.2})Zr_2O_{7+x}$ pyrochlore. In $Nd_2Zr_2O_7$, Zr is surrounded by six oxygens and in $(Zr_{0.84}Y_{0.16})O_{1.92}$ by 7.6 oxygen atoms, assuming that *Y* is eightfold coordinated at this *Y* content [33]. The oxidised $(Nd_{1.8}U_{0.2})Zr_2O_{7+x}$ pyrochlore reveals the highest O/An ratio of the investigated samples. If the additional oxygen atoms exclusively increase the Zr–O coordination number, Zr is surrounded by 6.6 oxygens in this sample. The XANES of these three samples are quite different in the region of the white line. Two peaks (A, B) have nearly the same intensity for $(Zr_{0.84}Y_{0.16})O_{1.92}$, but peak B is more intense for $Nd_2Zr_2O_7$ and shifted to higher energies. The Zr *K*-edge XANES of oxidised $(Nd_{1.8}U_{0.2})Zr_2O_{7+x}$ is generally similar to that of the pure $Nd_2Zr_2O_7$ pyrochlore. However, there is some correspondence to that of $(Zr_{0.84}Y_{0.16})O_{1.92}$ as peak A exhibits a small increase in intensity, whereas peak B shifts to lower energy and decreases slightly in intensity. These features in the Zr *K*-edge XANES structure of oxidised $(Nd_{1.8}U_{0.2})Zr_2O_{7+x}$ indicate a change in the local Zr structure, which is attributed to an increase of the average Zr–O coordination number so that the oxygen atoms added to the pyrochlore by the actinide dopant's are preferentially associated with Zr.

3.4. EXAFS

The k^3-weighted experimental EXAFS and Fourier transforms (FT's) of the Zr *K* and actinide L_3-edges are shown in Fig. 4. For comparison the Zr *K*- and Nd L_3-edges of neodymium pyrochlore $Nd_2Zr_2O_7$ are also given. The FT of the Zr *K*-edge EXAFS reveals two peaks at 1.8 and 3.7 Å (R+Δ) and is similar for all samples. The first peak corresponds to a shell of six oxygen atoms (48*f*) at a distance of 2.1 Å. The second peak is due to a shell of 12 metal atoms (comprising 6 Zr_1+5.4 Nd_1+0.6 An_1), which have the same crystallographic interatomic distance, but different backscattering amplitudes and phase shifts. Due to the low concentration of the *An* atoms, the second FT peak was modelled with 6 Zr_1 and 6 Nd_1 atoms. The evaluation of the calculated theoretical backscattering amplitudes and phase shifts indicates that a four-legged MS path along the collinear Zr–O–Zr–O′ (4.2 Å) is significant in amplitude and its inclusion in the fitting procedure improved the fit quality mainly at lower *k*-values. Anion disorder by partial filling the unoccupied 8*a* oxygen site was reported for a $Gd_2(Ti_{1-x}Zr_x)_2O_7$ pyrochlore [13]. Furthermore, oxygen induced by the actinide dopants could preferential fill the unoccupied 8*a* oxygen site of the pyrochlore structure. Therefore, the Zr *K*-edge EXAFS data were also fit with a structural model including an additional oxygen shell at a Zr–O_{8a} distance of 2.3 Å. Approximately one oxgyen atom was detected at a Zr–O_{8a} distance of 2.25–2.30 Å, independent of the actinide dopant and its oxidation state. However, the fit was improved only marginal in quality and this additional oxygen shell contributes too little to derive meaningful structural parameters. The absence of a considerable oxygen antisite disorder in these $(Nd_{1.8}An_{0.2})Zr_2O_{7+x}$ pyrochlore agrees with the observed presence of the MS along Zr–O–Zr–O′.

The FT's of the Nd and actinide L_3-edges EXAFS are less similar for the different samples. The FT of the Nd L_3-edge in $Nd_2Zr_2O_7$ consists of several peaks between 1.5 and 6 Å (*R*+Δ). The first two peaks represent the eight oxygen atoms surrounding the Nd at distances of 2.31 Å (O_{8b}, $N = 2$) and 2.58 Å (O_{48f}, $N = 6$). As for Zr, the Nd is surrounded by 12 metal atoms at 3.77 Å (6 Zr_1+6 Nd_1 in $Nd_2Zr_2O_7$). The more distant FT peaks represent 12 oxygens at 4.32 Å (O_3) and six Zr atoms at 5.34 Å (Zr_2). MS along Nd–O–Nd–O′ is not relevant, as the paths are degenerate due to the split O_{8b}/O_{48f} shells. Comparing the FT of the Nd L_3-edge EXAFS with those of the actinide's, the FT's of the U and Am samples treated in Ar/H_2 are most similar to the Nd data. Uranium(IV) and Am(III) have ionic radii close to Nd. However, as the FT peaks result from overlapping backscattering paths and destructive interference [13], only limited conclusion can be derived from visual FT inspection. The experimental Nd and actinide EXAFS data were fitted using a structural model based on a Nd cluster as in $Nd_2Zr_2O_7$ (O_{8b}, O_{48f}, Nd_1, Zr_1, O_3, Zr_2). The O_3 and Zr_2 shells were included in the fit, since overlapping FT peaks do not allow an

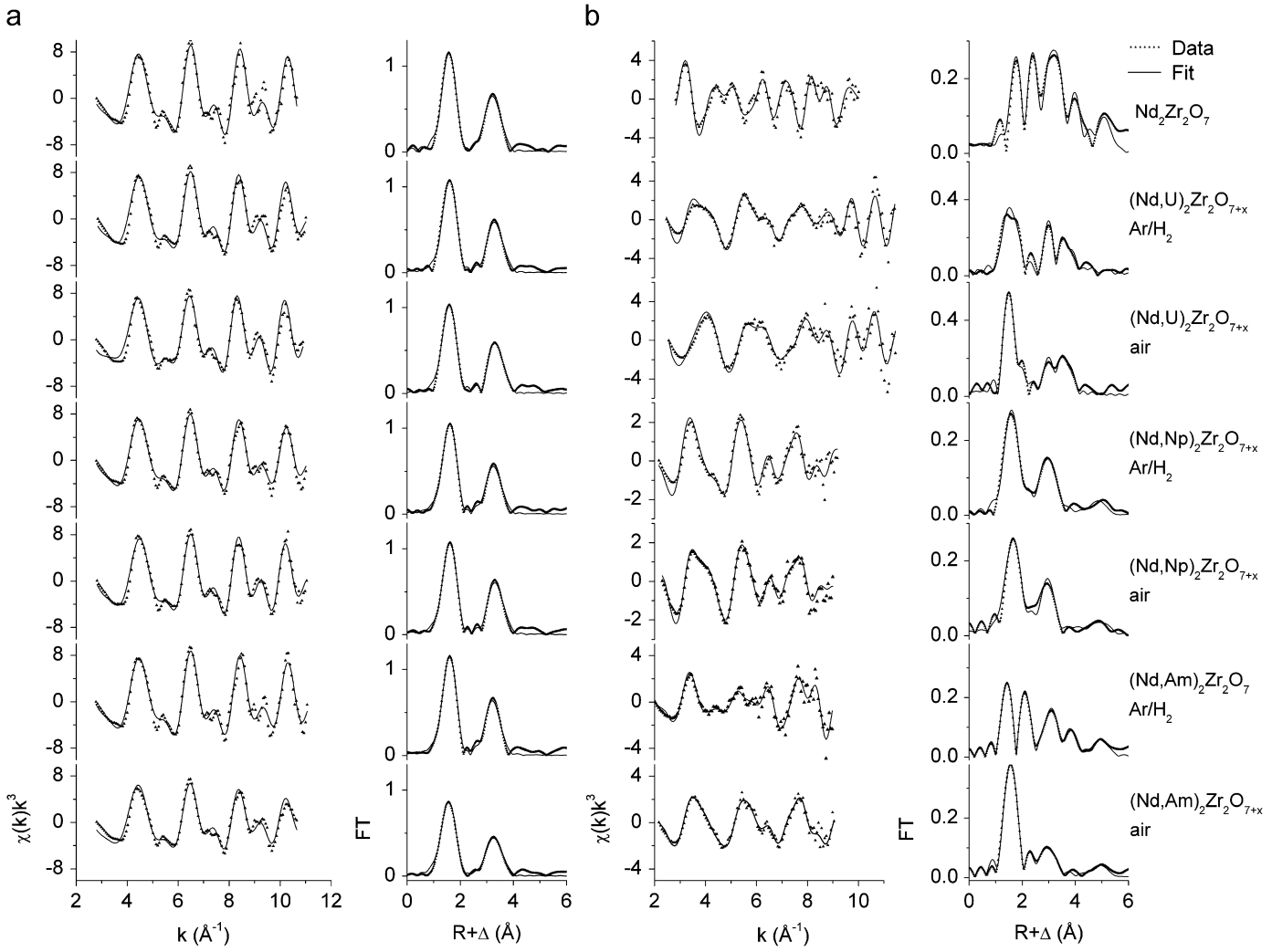

Fig. 4. Fourier transformed k^3-weighted $\chi(k)$ data of the (left) Zr *K*-egde and of (right) Nd, U, Np, Am L_3-edge in the $(Nd_{1.8}An_{0.2})Zr_2O_{7+x}$ pyrochlore.

accurate FT filtering. The coordination numbers (N) were held constant at the crystallographic values. In the case of the oxidised U sample, inclusion of the O_3 and Zr_2 shells did not improve the fit and were neglected for this sample. The introduction of a third cummulant term for the O_{48f} atoms significantly improves the fit for the actinide EXAFS data, but not the fit of the Nd and Am(III) EXAFS. Thus a non-Gaussian distribution of the O_{48f} atoms around the actinides in the doped material is indicated. Similar observations are reported for distorted fluorite structures [34,35]. Attempts to fit a single oxygen shell surrounding the actinides—i.e. a structural environment like Zr in $Nd_2Zr_2O_7$—failed, as the obtained shift in ionisation energy resulted in an unacceptable negative value of ΔE_0 (>-15 eV) determined from the maxima of the first derivate XANES. Furthermore, there was no indication of a predominant An–O–An–O′ multiple scattering path as observed for the Zr *K*-edge data.

The refined distances between the Zr, Nd, An and their surrounding oxygen atoms (i.e. nearest neighbours) are plotted in Fig. 5 versus the actinide ionic radii. The complete set of structural parameters is provided as supplementary data. The Zr–O, Nd–O_{8b}, and Nd–O_{48f} distances are plotted with error bars calculated from the difference of EXAFS values for $Nd_2Zr_2O_7$ and the distances from the crystal structure of $Nd_2Zr_2O_7$ [8]. The error bars for the Nd–O_{8b} and Nd–O_{48f} distance are larger than the usual error in determining interatomic distances by EXAFS spectroscopy (0.01–0.02 Å). This is mainly due to the difficulty to separate backscattering paths with nearly the same distance, such as Nd–O_{8b} and Nd–O_{48f} in the pyrochlore structure [13].

The Zr–O bond distances in the $(Nd_{1.8}An_{0.2})Zr_2O_{7+x}$ pyrochlore are in the range between 2.09 and 2.11 Å. Any small increase in the Zr–O bond length with decreasing ionic radii (i.e. higher *An* oxidation state) of the dopant is close to the experimental error (0.01 Å). This behaviour could be expected, if oxygen atom incorporation in the $(Nd_{1.8}An_{0.2})Zr_2O_{7+x}$ pyrochlore structure due to heterovalent dopant's is mainly associated with the Zr atoms, increasing the mean Zr–O coordination number. However, the amount of Zr host atoms is 10 times higher than the *An* dopant, reducing the impact of additional oxygen on the Zr–O distance. In addition, the induced oxygen atoms could occupy the vacant 8*a* site at a larger distance of 2.3 Å, but this is difficult to detect by EXAFS analysis due to the low occupancy of the site. Further investigations using ^{17}O MAS–NMR are planned to elucidate the location of these excess O atoms.

The two nearest neighbor *An*–O bond distances show a linear dependence on the ionic radii of the dopant ions. With increasing ionic radius both *An*–O_{8b} and *An*–O_{48f} distances increase, while the difference (splitting) between *An*–O_{8b} and *An*–O_{48f} remains nearly constant. This clearly indicates that the actinides are accommodated in the structural Nd site in the $(Nd_{1.8}An_{0.2})Zr_2O_{7+x}$ pyrochlore and that the *An*–O bond length causes most of the

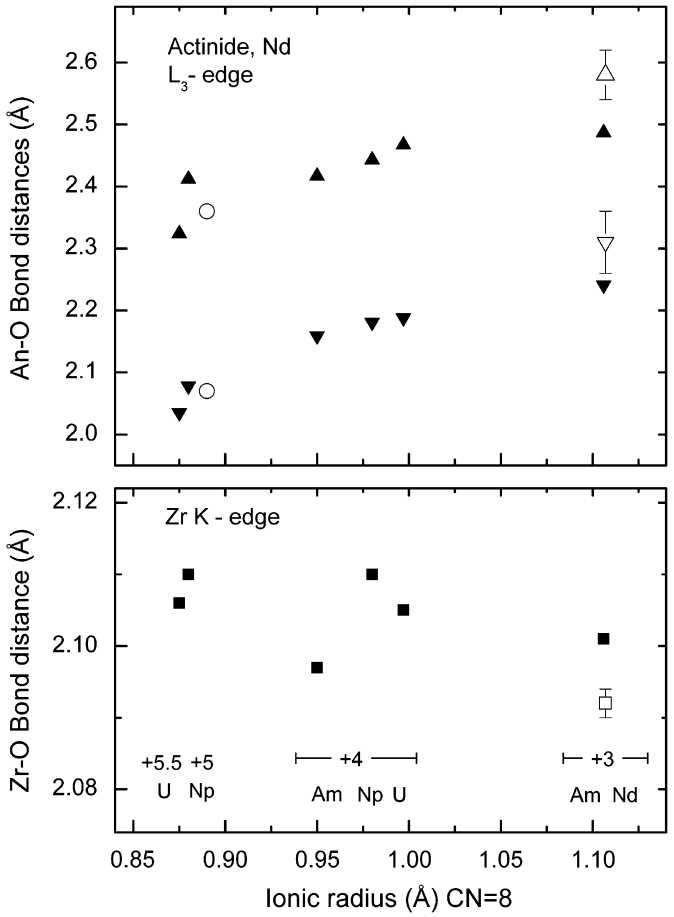

Fig. 5. Zr–O (■), *An*–O_{8b} (▼), and *An*–O_{48f} (▲) bond distances in the $(Nd_{1.8}An_{0.2})Zr_2O_{7+x}$ pyrochlore. U(V)–O (○) bond distances in a Ca–Gd–Pu–U titanate pyrochlore/zirconolite [17]. The error bar given for the Zr–O (⩽), Nd–O_{8b} (▽), and Nd–O_{48f} (△) bond distances in $Nd_2Zr_2O_7$ refers to the difference of the values calculated from the crystal structure and those obtained by EXAFS.

lattice parameter contraction with decreasing *An* ionic radii. The average *An*–O bond distances (*N*-weighted average) are close to the bond distances expected from the ionic radii in structurally related AnO_2 compounds. For example, the average U(IV)–O bond length is 2.40 Å in $(Nd_{1.8}U_{0.2})Zr_2O_{7.1}$ and 2.37 in UO_2. Obviously the actinides preserve their specific bond distances to some extend once incorporated in the pyrochlore, similar to dopant ions in stabilised zirconia (defect fluorite structure). The resulting misfit of the smaller actinide ions in the Nd site displaces the oxygen atoms and a non-Gaussian *An*–O_{48f} distribution was found by the need of a third cummulant term to fit the experimental *An* EXAFS data.

4. Discussion

There is little available information about UO_2–UO_3 solid solutions with stabilised zirconia. UO_2 forms a continuous solid solution with Ca stabilised zirconia [36]. During oxidation of $(Ca_{0.23}Zr_{0.77})O_2$–UO_2 solid solutions ($U<0.3$) in air the O/U ratio rises from 2.0 to approximately 2.35 [37]. This corresponds to a mixed U(IV) and U(V) valency. Spectroscopic evidence for U(IV) oxidation to U(V) is reported for U doped zirconolite, $CaU_xZr_{1-x}Ti_2O_7$ [16], when the material, initially sintered in Ar, was heated in air at 1400 °C. Fortner et al. [17] reported a $A_2Ti_2O_7$ (*A*: Ca+Gd+Pu+U) titanate pyrochlore (sintered at 1350 °C in Ar) with uranium mainly in the pentavalent oxidation state. Based on the short U(V)–O distance (3–4 O at 2.07 Å and 3–4 O at 2.36 Å) they concluded that U(V) preferentially occupies the octahedral Ti site in this pyrochlore. However, uranium (V) has a much smaller ionic radius (e.g. U(V): 0.89 Å) than the eightfold coordinated *A* atoms in pyrochlore (e.g. Ca: 1.12 Å, Nd: 1.11 Å, Gd: 1.05 Å). In stabilised zirconia such differences in the ionic radii are generally preserved and the dopant–oxygen bond lengths are characteristic of the particular dopant ion [12]. Accordingly, the *An*–O bond distances in pyrochlore measured by EXAFS should differ from the metal–oxygen distances calculated from bulk crystal structure (e.g. Nd–O or Ca–O). Indeed, the determined *An*–O distances in $(Nd_{1.8}An_{0.2})Zr_2O_7$ correlate with the dopant ionic radii (Fig. 5). As found by the EXAFS analyses in this study, uranium prefers the eightfold coordinated Nd site in the $(Nd_{1.8}U_{0.2})Zr_2O_7$ pyrochlore, as is indicated by the splitting of the *An*–O distances, a characteristic for the eightfold coordination in pyrochlore. A less-distorted and single *An*–O distance would have been expected if the actinides had occupied the octahedral site. Furthermore, taking 0.89 Å as an estimate for the U(V) ionic radius (as for Np, see above), the U–O bond lengths reported by Fortner et al. [17] fit exactly the *An*–O bond lengths of the $(Nd_{1.8}An_{0.2})Zr_2O_{7+x}$ pyrochlore shown in Fig. 5. This might suggest that U(V) could occupy the eightfold coordinated *A* site in this titanate pyrochlore [17], and not as originally thought the octahedral *B* site.

The incorporation of Np in yttria stabilised zirconia (YSZ, 14.3 mol% $YO_{1.5}$) has been reported following preparation both in reducing (Ar/H_2, 1500 °C) and oxidising sinter atmosphere (air, 1500 °C) [38]. A single fluorite structure forms and the lattice parameter is independent of the sintering atmosphere, indicating that Np incorporated in YSZ is tetravalent both in reducing and oxidising conditions. These findings are in contrast to the present study, where Np is oxidised to Np(V) at 800 °C. The main difference between (defect) fluorite and pyrochlore structure is the availability of oxygen vacancies. In YSZ, oxygen vacancies, induced by the Y atoms, are associated with the Zr atoms and the Zr coordination number is approximately 7.7 for 14.3 mol% $YO_{1.5}$. As hyperstoichiometric NpO_{2+x} is not known [24], any oxygen introduced during Np oxidation would need to be accepted by the O vacancies created by the Y(III). The average Zr coordination number should rise if Np is oxidised to Np(V) and, in addition, the oxygen vacancies are filled up. Consequently, Np oxidation is hindered in YSZ by the low availability of oxygen vacancies, which is essentially caused by the low Y content in YSZ. If the $(Nd_{1.8}An_{0.2})Zr_2O_{7+x}$ pyrochlore is viewed as deviation of the fluorite structure, then there are many more available (ordered, 8*a* site) oxygen vacancies associated to Zr. Thus, Np oxidation is not hindered by the limited number of vacancies and Np(V) is observed after oxidation. A similar effect is reported for the ternary oxide $(Nd,Np)O_2$ system, where the Np valence increase from +5 in $(Nd_{0.5}Np_{0.5})O_2$ to +6 in $(Nd_{0.67}Np_{0.33})O_2$ [39].

The oxidation state of Pu and Am in $(Nd_{1.8}An_{0.2})Zr_2O_7$ is +3 under reducing and +4 under oxidising conditions. This can be expected from the existence of the isostructural $Pu_2Zr_2O_7$, $Am_2Zr_2O_7$ pyrochlores [6], and the structurally related PuO_2 and AmO_2 fluorites. Both Pu(III) and Am(III) occupy the eightfold coordinated *A* site in the pyrochlore studied here. During their oxidation in air at 800 °C, Am(IV) remains in this coordination as indicated from the Am L_3-edge EXAFS measurement. Compared with the other tetravalent actinides U(IV), Np(IV), and Am(IV), it can also be assumed that Pu(IV) is coordinated in eightfold coordination. Atomistic calculations suggest that Pu(IV) prefers the octahedral and U(IV) a mixed coordination in $Nd_2Zr_2O_7$ [40], unfortunately the stoichiometric assumption made for these calculations are different compared to the $(Nd_{1.8}An_{0.2})Zr_2O_{7+x}$ pyrochlore, which allows no meaningful comparison. As for the U and Np samples the excess oxygen in the Am(IV) and Pu(IV)

containing pyrochlores of this study is most probably accomodated around the Zr atoms.

5. Conclusion

A series of actinides (Th, U, Np, Pu, Am, and for comparison La and Nd) were incorporated in a $(Nd_{1.8}An_{0.2})Zr_2O_{7+x}$ pyrochlore. The valence of the actinides was varied by the sintering atmosphere. Sintering in Ar/H_2 at 1600 °C (reducing conditions) leads to Th(IV), U(IV), Np(IV), Pu(III), and Am(III). After annealing in air at 800 °C (oxidising conditions), the oxidation states are changed to Np(V), Pu(IV), Am(IV), and for uranium to a mixed U(V)–U(VI) valancy. The lattice parameter of the $(Nd_{1.8}An_{0.2})Zr_2O_{7+x}$ pyrochlore shows a linear dependence on the ionic radii of the actinide ions. A split next nearest neighbour oxygen shell around the actinides, similar to that surrounding of Nd, was found by EXAFS. The obtained *An*–O bond distances also correlate with the actinide ionic radii, clearly indicating that these actinides occupy the Nd site in $(Nd_{1.8}An_{0.2})Zr_2O_{7+x}$. Obviously, incorporated actinides maintain their own (average) *An*–O bond distances. However, they accept the surrounding structural environment of the host matrix, i.e. the characteristic splitting into a shorter and longer *An*–O bond distance is found at characteristic distances of the dopant ions. This conclusion could well be valid for the isostructural titanate pyrochlores.

The heterovalent substitution of Nd(III) with actinides is possible, because additional oxygens introduced with the actinides can be accommodated in the unoccupied oxygen site in the pyrochlore structure. The high number (25%) of unoccupied oxygen sites in pyrochlore compared to stabilised zirconia has an impact on the suitability of pyrochlores (either zirconia or titanate based) as a conditioning matrix. A significant oxidation of Np was found in the $(Nd_{1.8}Np_{0.2})Zr_2O_{7+x}$ pyrochlore. The susceptibility of Np(IV) oxidation is much less in stabilised zirconia, where less oxygen vacancies are present due to the lower amount of trivalent stabilisers.

Acknowledgements

We would like to acknowledge the assistance of D. Bouexière, H. Hein, M. Holzhäuser and C. Boshoven in the preparation of samples, and thank the Ångströmquelle Karlsruhe, ANKA, for providing beamtime for the EXAFS measurements.

Appendix A. Supplementary material

Supplementary data associated with this article can be found in the online version at 10.1016/j.jssc.2008.09.017.

References

[1] A. Fernández, D. Haas, R.J.M. Konings, J. Somers, J. Am. Ceram. Soc. 85 (2002) 694–696.
[2] Y. Croixmarie, E. Abonneau, A. Fernández, R.J.M. Konings, F. Desmoulière, L. Donnet, J. Nucl. Mater. 320 (2003) 11–17.
[3] S. Lutique, D. Staicu, R.J.M. Konings, V.V. Rondinella, J. Somers, T. Wiss, J. Nucl. Mater. 319 (2003) 59–64.
[4] S.X. Wang, B.D. Begg, L.M. Wang, R.C. Ewing, W.J. Weber, K.V. Govidan Kutty, J. Mater. Res. 14 (1999) 4470–4473.
[5] G.R. Lumpkin, Elements 2 (2006) 365–372.
[6] R.G. Haire, P.E. Raison, Z. Assefa, J. Nucl. Sci. Technol. (Supp. 3) (2002) 616–619.
[7] R.C. Ewing, W.J. Weber, J. Lian, J. Appl. Phys. 95 (2004) 5949–5971.
[8] E.J. Harvey, K.R. Whittle, G.R. Lumpkin, R.I. Smith, S.A.T. Redfern, J. Solid State Chem. 178 (2005) 800–810.
[9] N.K. Kulkarni, S. Sampath, V. Venugopal, J. Nucl. Mater. 281 (2000) 248–250.
[10] S. Yamazaki, T. Yamashita, T. Matsui, T. Nagasaki, J. Nucl. Mater. 294 (2001) 183–187.
[11] D. Komyoji, A. Yoshiasa, T. Moriga, S. Emura, F. Kanamaru, K. Koto, Solid State Ionics 50 (1992) 291–301.
[12] P. Li, I.-W. Chen, J.E. Penner-Hahn, J. Am. Ceram. Soc. 77 (1994) 118–128.
[13] N.J. Hess, B.D. Begg, S.D. Conradson, D.E. McCready, P.L. Gassman, W.J. Weber, J. Phys. Chem. B 106 (2002) 4663–4677.
[14] R.B. Greegor, F.W. Lytle, R.J. Livak, F.W. Clinard Jr., J. Nucl. Mater. 152 (1988) 270–277.
[15] F. Farges, R.C. Ewing, G.E. Brown Jr., J. Mater. Res. 8 (1993) 1983–1995.
[16] E.R. Vance, G.R. Lumpkin, M.L. Carter, D.J. Cassidy, C.J. Ball, R.A. Day, B.D. Begg, J. Am. Ceram. Soc. 85 (2002) 1853–1859.
[17] J.A. Fortner, A.J. Kropf, R.J. Finch, A.J. Bakel, M.C. Hash, D.B. Chamberlain, J. Nucl. Mater. 304 (2002) 56–62.
[18] P. Villella, S.D. Conradson, F.J. Espinosa-Faller, S.R. Foltyn, K.E. Sickafus, J.A. Valdez, Phys. Rev. B 64 (2001) 104101.
[19] M. Walter, C. Nästren, J. Somers, R. Jardin, M.A. Denecke, B. Brendebach, J. Solid State Chem. 180 (2007) 3130–3135.
[20] J. Rodriguez-Carvajal, FULLPROF version 3.00, ILL, Grenoble, 2004, unpublished.
[21] J. Rothe, M.A. Denecke, K. Dardenne, T. Fanghänel, Radiochim. Acta 94 (2006) 691–696.
[22] T. Ressler, J. Synchrotron Rad. 5 (1998) 118–122.
[23] A.L. Ankudinov, B. Ravel, J.J. Rehr, S.D. Conradson, Phys. Rev. B 58 (1998) 7565–7576.
[24] L.R. Morss, N.M. Edelstein, J. Fuger, The Chemistry of the Actinide and Transactinide Elements, Springer, Dordrecht, 2006.
[25] R.D. Shannon, Acta Crystallogr. A 32 (1976) 751–767.
[26] F. David, J. Less-Common Met. 121 (1986) 27–42.
[27] W.J. Weber, R.C. Ewing, C.R.A. Catlow, T. Diaz de la Rubia, L.W. Hobbs, C. Kinoshita, H.J. Matzke, A.T. Motta, M. Natasi, E.K.H. Salje, E.R. Vance, S.J. Zinkle, J. Mater. Res. 13 (1998) 1434–1484.
[28] J. Lian, L. Wang, J. Chen, K. Sun, R.C. Ewing, J. Matt Farmer, L.A. Boatner, Acta Mate. 51 (2003) 1493–1502.
[29] Y. Liu, L. Withers, L. Norén, J. Solid State Chem. 177 (2004) 4404–4412.
[30] A.V. Soldatov, D. Lamoen, M.J. Konstantinovic, A.C. Scheinost, M. Verwerft, J. Solid State Chem. 180 (2007) 54–61.
[31] M.A. Denecke, Coord. Chem. Rev. 250 (2006) 730–754.
[32] E.A. Hudson, J.J. Rehr, J.J. Bucher, Phys. Rev. B 52 (1995) 13815–13826.
[33] P. Li, I.-W. Chen, J.E. Penner-Hahn, Phys. Rev. B 48 (1993) 10074–10081.
[34] S. Lemaux, A. Bensaddik, A.M.J. van der Erden, J.H. Bitter, D.C. Koningsberger, J. Phys. Chem. B 105 (2001) 4810–4815.
[35] P. Martin, S. Grandjean, C. Valot, G. Carlot, M. Ripert, P. Blanc, C. Hennig, J. Alloys Compd. 444–445 (2007) 410–414.
[36] J.H. Handwerk, G.D. White, D.C. Hill, J. Am. Ceram. Soc. 46 (1963) 29–32.
[37] N.K. Kulkarni, S. Sampath, V. Venugopal, Ceram. Int. 27 (2001) 839–846.
[38] H. Kinoshita, K. Kuramoto, M. Uno, T. Yanagi, S. Yamanaka, H. Mitamura, T. Banba, J. Am. Ceram. Soc. 83 (2000) 391–396.
[39] C. Keller, A. Boroujerdi, J. Inorg. Nucl. Chem. 34 (1972) 1187–1193.
[40] A. Cleave, R.W. Grimes, K. Sickafus, Philos. Mag. 85 (2005) 967–980.